Chinese Journal of
POLYMER SCIENCE

RESEARCH ARTICLE

https://doi.org/10.1007/s10118-025-3405-8
Chinese J. Polym. Sci. **2025**, *43*, 2138–2149

Tube Model for Complex Polymer Knots

Jian-Song Yang[a,†], Yong-Jian Zhu[a,†], Qi-Yuan Qiu[a], Wen-Xuan Xu[a], and Liang Dai[a,b*]

[a] *Department of Physics, City University of Hong Kong, Hong Kong 999077, China*
[b] *Shenzhen Research Institute, City University of Hong Kong, Shenzhen 518057, China*

Electronic Supplementary Information

Abstract Knotting occurs in polymers and affects polymer properties. Physical understanding of polymer knots is limited due to the complex conformational space of knotted structures. The knotting problem can be handled by the tube model, which assumes that knotted polymer segments are confined in a virtual tube. Recently, we quantified this virtual tube using a computational algorithm. The algorithm was limited to the simplest knot: 3_1 knot. It remains unclear how the tube model and computational algorithm are applied to more complex knots. In this work, we apply the tube model to 4_1, 5_1, and 5_2 knots, resulting in several findings. First, the computational algorithm developed for 3_1 knot cannot be directly applied to 4_1 knot. After modifying the algorithm, we quantify the tubes for 4_1 knot. Second, we find that, for all four knot types, the knot-core region have less average bending energy density than unknotted regions when the chain bending stiffness is small. This counterintuitive result is explained by the tube model. Third, for all four knot types, polymer segments at the boundaries of knot cores adopt nearly straight conformations (almost zero bending) and exhibit lower local bending compared to other knot-core regions and unknotting regions. This local behavior is also consistent with prediction from the tube model. This counterintuitive result is also explained by the tube model. Fourth, for all four knot types, when a polymer has non-uniform bending stiffness, a knot prefers certain chain positions such that the knot boundary locates at one stiff segment. Overall, our work paves the way for applying the tube model to complex polymer knots and obtains many common results for different knot types, which can be useful in understanding many knotting systems, such as DNA knots *in vivo*.

Keywords Polymer knot; Tube model; Monte Carlo simulation; Molecular dynamics; Knot type

Citation: Yang, J. S.; Zhu, Y. J.; Qiu, Q. Y.; Xu, W. X.; Dai, L. Tube model for complex polymer knots. *Chinese J. Polym. Sci.* **2025**, *43*, 2138–2149.

INTRODUCTION

The uncrossability of polymer segments causes polymer entanglements, which dramatically affect polymer properties.[1,2] Entanglement is one key reason why some polymer properties are fundamentally different from small molecules. There are two types of entanglements: inter-chain entanglements and intra-chain entanglements. The inter-chain entanglements are common for polymer solutions at high concentrations,[3] and polymer melts.[4,5] Intra-chain entanglements, often in the form of knotting,[6–10] occur in dilute solutions of long polymers, such as DNA solutions used in many polymer physics experiments.[11–21] Inter-chain entanglements have been extensively investigated in the past decades, while the understanding of polymer knotting is relatively less.

Knotting affects many properties, including mechanical, rheological, chemical, biological and crystallization and amorphous properties.[22] Knotting can reduce the minimum force of breaking a polymer,[23–25] and slow down polymer conformation relaxation,[11] and stretching kinetics.[12,26] Knotting greatly affects polymer nanopore translocation and viral ejection of DNA, such as jamming the translocation process.[13,16,20,27–31] Knotting can facilitate the catalysis of a manmade knotted molecule,[32] and a knotted protein.[33] Knotting also affects polymer crystallization,[34,35] and glass formation.[36]

While many intriguing phenomena have been observed, theoretical understanding of polymer knots is limited. Tackling the polymer-knot problem from a statistical physics perspective is challenging, because deriving the conformational entropy of a polymer knot requires knowing the polymer conformational space of a given knot type, which is very irregular and hard to obtain.

Previous studies have found that the tube model, which was originally developed for inter-chain entanglements,[1,2] can be applied to polymer knots with some modifications.[37–39] The original idea of the tube model for polymer knots was proposed three decades ago by Grosberg and co-workers.[39] The idea of the tube model is that entanglements restrict the moving path of a polymer and produce a virtual tube that confines a polymer. The effects of entanglements on polymer conformations and dynamics can be considered through tube confinement. In the tube model for polymer knots, the polymer segments in the knot core are as-

* Corresponding author, E-mail: liangdai@cityu.edu.hk
† These authors contributed equally to this work.
Received June 9, 2025; Accepted June 27, 2025; Published online September 10, 2025

sumed to be confined in a virtual tube.

Our recent studies constructed this virtual tube using an algorithm:[40,41] (i) superimpose many knot-core conformations; (ii) then calculate the average knot-core shape of these conformations; (iii) lastly, calculate the fluctuations of individual conformations around the average shape. The average shape corresponds to the tube axis and the fluctuations correspond to the tube diameters. It is worth pointing out that for polymer knots, the virtual tubes usually have fixed shapes. For comparison, in the case of inter-chain entanglements, the virtual tubes usually have no fixed shape. In this respect, the idea of the tube model works even better for polymer knots, because the corresponding virtual tubes have well-defined shapes and can be visualized.

Constructing the tubes for polymer knots enables us to understand many properties of polymer knots, including the shapes, bending energies, and conformational entropy.[31,42–45] In particular, the tube model can clearly explain one counterintuitive phenomenon: knotting often reduces polymer bending energy.[42] The reason is that tube confinement can suppress the polymer bending caused by thermal fluctuation.

Previous studies have constructed the tube model for only one knot type: 3_1 knot. Applying the tube model to other complex knots is not trivial, because the algorithm of quantifying the tube depends on the knot type. Directly applying the existing algorithm to 4_1 knot gives a wrong tube,[40] which will be elaborated in this work.

In this work, we develop a new algorithm to quantify the knot tubes for complex knots. Based on the knot tubes, we obtain and explain several common properties of different knot types.

METHODS

Monte Carlo Simulation

We obtain equilibrium knot conformations by Monte Carlo (MC) simulations, similar to our previous studies.[40,41] In the MC simulations, a ring polymer is described by a string of touching beads (Fig. 1). The polymer length is L=300 in most simulations. The bond length between adjacent beads is fixed as a, which is treated as the unit length in this work. We implement purely hardcore repulsion for all bead-bead pairs. The bending energy for three adjacent beads is described by

$$E_{\text{bend}}/(k_{\text{B}}T) = (1/2)\kappa\theta^2 \text{ with } \kappa = L_{\text{p}}/a \quad (1)$$

where θ is the bending angle, k_{B} is the Boltzmann constant, and T is the temperature. The bending stiffness is tuned by κ, which determines the persistence length L_{p}. In our simulations, the temperature is fixed as T=1 and $k_{\text{B}}T$ serves as unit energy, and so the persistence length L_{p} is directly linked to the chain bending stiffness κ.

Each simulation starts with a ring conformation with the desired knot type, such as 4_1, 5_1, or 5_2. In each MC step, we randomly select a bead and perform a crankshaft move for this bead, *i.e.*, rotating this bead along the axis formed by two adjacent beads. The rotation angle is a random value between 0 and 2π. We purposefully use this local move to avoid the inter-penetration of polymer segments so that the knot type is preserved during the simulation. Hence, these simulations can output equilibrium conformations of given knot types. We typically run 10^{10} steps for each MC simulation and save the conformation every 10^4 steps for analysis. The number of MC steps is always at least 100 times more than the conformational correlation time estimated from the evolution of the radius of gyration. The correlation time is typically on the order of 10^7 steps.

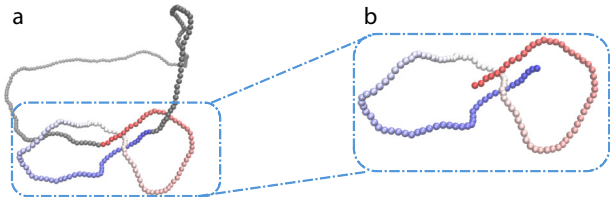

Fig. 1 Conformation of a knotted polymer: (a) our Monte Carlo simulation snapshot of a polymer ring containing a 4_1 knot; (b) knot core.

Knot Analysis

We determine the knot type for a give conformation using the Alexander polynomials.[46,47] To determine the knot core, we cut beads one by one from both ends until the knot type changes (Fig. 1). The knot size, L_{knot}, is defined as the contour length of the knot core. In the calculation of knot-core regions, we need to determine the knot type for an open chain conformation. We employ the minimally interfering closure scheme to connect chain ends before the calculation of the Alexander polynomials.[48] This end closure scheme appears to be a very reasonable way to close ends, and has been widely used in our previous studies.[31,40–43,45] We have also tried the end closure by straight line, which does not affect the conclusions of this work (See Figs. S6 and S7 in the electronic suppplementary information, ESI).

Constructing the Tube for 4_1 Knots Using the Traditional Method

Similar to the previous method,[40] we attempt to average a large number of knot-core conformations of a given knot-size to obtain the shape of 4_1 knots (Figs. 2a–2c). From simulations, we select knot-core conformations of a given knot size, *e.g.*, L_{knot}=100a. Before averaging, we translate and rotate the knot-core conformations to minimize the deviations among them. However, the average conformation does not appear to be a 4_1 knot, because certain important structural features are cancelled out during averaging when the knot-core structures are not properly aligned. The result indicates that the traditional method does not work well for 4_1 knots. The reason will be described in the next subsection.

Problem in the Traditional Method

The problem with the traditional method can be exemplified by the first and second conformations in Fig. 2(b). Although both resemble each other, we cannot overlap them with rotation. We find that we can overlap them by mirror reflection, as shown by the first and second conformations in Fig. 2(e).

A careful inspection of 4_1 knot conformations reveals that we can classify 4_1 knot conformations into eight types based on the position and direction of the first bead (Fig. 3). The first bead is indicated by red. The first conformation in Fig. 3(a) is labelled as $L\uparrow$, where L indicates that the first bead locates at the left side of the last bead, and ↑ indicates that the direc-

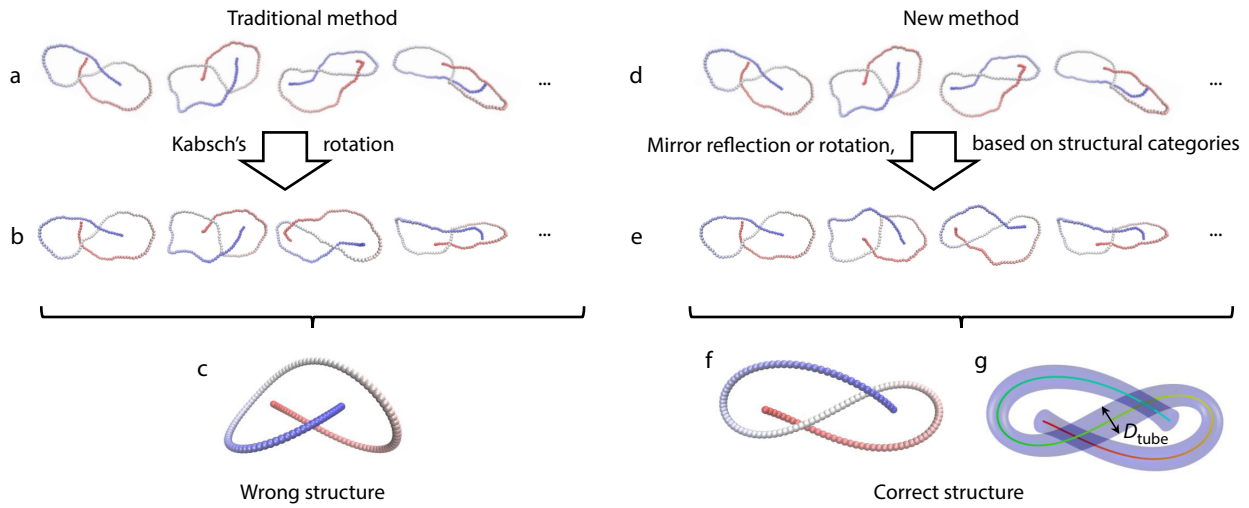

Fig. 2 Constructing the tube for 4_1 knots using the traditional method (a–c) and new method (d–g). In the traditional method, we translate and rotate many knot-core conformations (a) to minimize the deviations among them using the Kabsch algorithm and obtain the conformations in (b).[49] Then, we average the conformations in (b) and obtain the one in (c), which is apparently not a 4_1 knot. In the new method, we translate, rotate, and mirror-reflect the knot-core conformations (d) to minimize the deviations. The mirror-reflection will be described in the next Figure. Then, we average the conformations in (e) and obtain the one in (f). (g) A tube is displayed with the tube diameters corresponding to 0.2 times of root mean square fluctuation (RMSF). The scaling factor 0.2 is for better visualization.

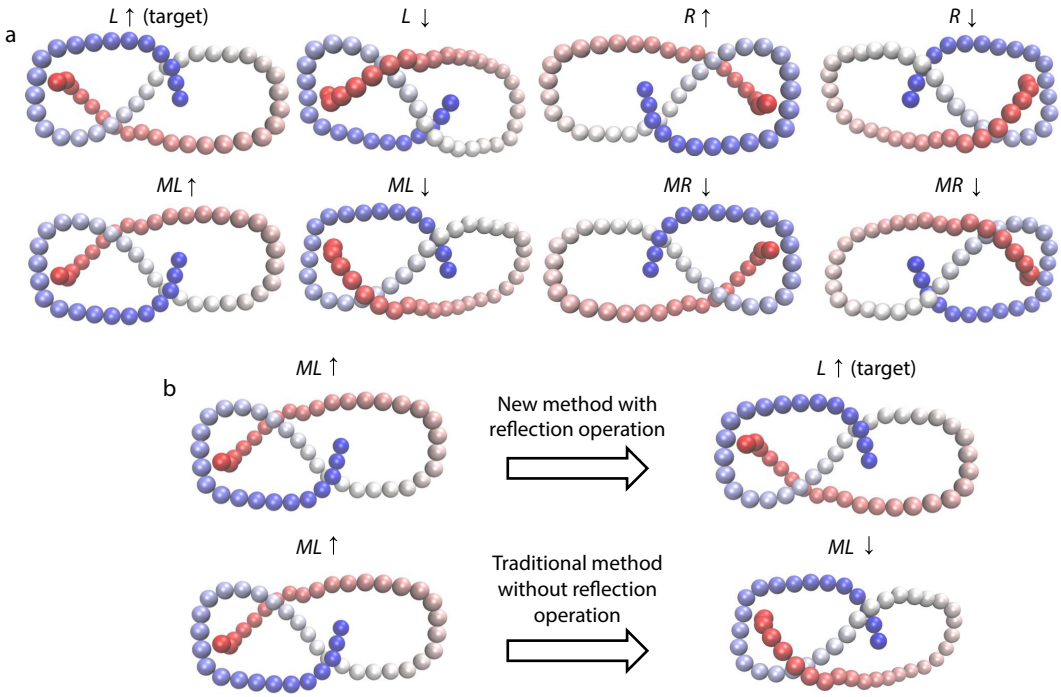

Fig. 3 Mirror reflection of knot conformation. (a) Classification of 4_1 knot conformations into 8 types based on the position and direction of the first bead (marked in red). The first conformation is labelled as $L\uparrow$, where L indicates that the first bead is located at the left side of the last bead, and ↑ indicates that the direction from the second bead to the first bead points outward of the plane of paper. R indicates right and ↓ indicates the direction points inward of the plane of paper. $ML\uparrow$, $ML\downarrow$, $MR\uparrow$, and $MR\downarrow$ are mirror reflections of $L\uparrow$, $L\downarrow$, $R\uparrow$, and $R\downarrow$, respectively. (b) The new method, including mirror reflection, can transform any knot conformation to the target type. The traditional method cannot do it. Note that before mirror reflections, each conformation is rotated to make the first and second principal axes aligning with x- and y- directions, respectively.

tion from the second bead to the first bead points outward of the plane of paper. Similarly, R indicates right, and ↓ indicates the direction points inward of the plane of paper. Note that before the classification, each conformation is rotated to make the first (longest) and second principal axes aligning with x- and y- directions, respectively.

In Fig. 3(a), the conformation $ML\uparrow$ is a mirror image of the conformation $L\uparrow$. Even though they share the same point and direction of the first bead, we cannot overlap them. Furthermore, we are unable to overlap them by rotation as

https://doi.org/10.1007/s10118-025-3405-8

shown in Fig. 3(b). This is the key reason why the traditional method fails to obtain the average 4_1 knot conformation.

Constructing the Tube for 4_1 Knots Using a New Method

After identifying the problem in the traditional method, we develop a new method to obtain the average 4_1 knot conformation. In addition to the translation and rotation, we add mirror-reflection to minimize the deviation among knot-core conformations (Figs. 2d and 2e). Basically, we transform all knot-core conformations toward $L\uparrow$. The conformations of $L\downarrow$, $R\uparrow$, and $R\downarrow$ can be transformed toward $L\uparrow$ through the rotation operation. The conformations of $ML\uparrow$, $ML\downarrow$, $MR\uparrow$, and $MR\downarrow$ can be transformed toward $L\uparrow$ through mirror-reflection and rotation. Then, we average the conformations in Fig. 2(e) and obtain the average 4_1 knot conformation one in Fig. 2(f). We also calculate the standard deviations of individual knot-conformations around the average conformation, which correspond to the half of tube diameters. Thus, the tube model is visualized in Fig. 2(g).

After aligning knot-core conformations through translation, rotation and mirror-flipping (as illustrated in Figs. 2d and 2e), we average these conformations to obtain the shape of knot, *i.e.*, the axis of the tube:

$$\begin{aligned} \vec{x}_{\mathrm{cen}}(k) &= \frac{1}{N_{\mathrm{conf}}}\sum_{\mathrm{i}=1}^{N_{\mathrm{conf}}}\vec{x}_{\mathrm{i}}(k) \\ R_{\mathrm{tube}}(k) &= \sqrt{\left[\frac{1}{N_{\mathrm{conf}}}\sum_{\mathrm{i}=1}^{N_{\mathrm{conf}}}\|\vec{x}_{\mathrm{i}}(k)-\vec{x}_{\mathrm{cen}}(k)\|^2\right]} \\ D_{\mathrm{tube}}(k) &\equiv 2R_{\mathrm{tube}}(k) \end{aligned} \tag{2}$$

Here, k=1, 2, ..., L_{knot} is the index of bead inside the knot-core, $\vec{x}_{\mathrm{i}}(k)$ is the 3D coordinate of the i^{th} bead in the k^{th} knot-core, and $\vec{x}_{\mathrm{cen}}(k)$ is the center of the knot-core conformation. R_{tube} and D_{tube} represent the radius and diameter of the tube, respectively. N_{conf} represents the total number of conformations.

Here we transform all knot-core conformations toward $L\uparrow$. If we transform toward $ML\uparrow$, then the final structure becomes mirror-reflection as well.

Molecular Dynamics Simulations of 4_1, 5_1, and 5_2 Knots

We also perform molecular dynamics simulations using the LAMMPS package,[50] in which a Langevin thermostat is applied,[44,51,52] to investigate the distribution of a knot in a polymer with non-uniform bending stiffness. The polymer conformation contains a knot, which can be a 4_1, 5_1, or 5_2 knot. Bead-bead interactions are described by the Weeks-Chandler-Andersen potential.[53] Typically, we run each simulation for 10^9 steps. We discard the first 10^8 steps and save the following conformations every 10^3 steps for the analysis of knot position.

RESULTS AND DISCUSSION

Tube Shape for 4_1 Knot

We construct the tube model for 4_1 knot using a new algorithm described in the method section. The old algorithm developed for 3_1 knot does not work for 4_1 knots, because 4_1 knot is achiral and rotation of 4_1-knotted conformations cannot align these conformations properly (Fig. 2a). After adding mirror-flipping operation (Fig. 3), we can align 4_1-knotted conformations properly (Fig. 2b).

Using the new algorithm, we obtain the tubes for 4_1-knotted conformations with different knot sizes (Fig. 4). See the knot-size distributions in Fig. S8 (in ESI). Because constructing these tubes requires a large number of knot-core conformations and huge computational cost of sampling chain conformations, we use a relatively short chain length $L = 300a$, which is shorter than our previous studies,[38,54] and does not cover the metastable knot size in long chains.

The tube axis corresponds to the average conformation, while the tube diameter, D_{tube}, corresponds to twice the standard deviation of individual conformations around the average conformation. Note that for better visualization, the tube diameters in Fig. 4 and the rest of figures are 0.2 times the actual tube diameters. If we use the original tube diameter, some parts of the tube overlap each other. Note that the tube diameter varies along the tube axis, because different sites of the knot structure have different fluctuations.

From Fig. 4, we can extract some quantities of tube shape. First, both ends of the knot are parallel but not in line. For comparison, a previous study obtained the tightest open 4_1 knot,[55] where the two ends are parallel and in line. Such difference is not surprising, because our 4_1 knot conformations are relaxed, while the tightest 4_1 knot is under a strong pulling force. We calculate the angle formed between the tangent at the knot-core boundaries and the *x*-*y* plane, which ranges from 40° to 70° (see Fig. S1 in ESI).

Second, both knot-core boundaries locate in the two loops formed in the knot. If the segments at knot-core boundaries want to optimize the translational entropy, the average location of the knot core boundaries would be at the center of loop (Fig 4a). We notice that the actual knot-core boundaries location deviate from the loop center. Such deviation can reduce the overall bending energy of knot, as pointed out by our previous study for the average conformation of 3_1 knot.[40]

Third, the average conformation is quite flat. The flatness can be quantified by the ratio of the maximum span in *z* direction (the shortest principal axis of conformation) to the one in *x* direction (the longest principal axis). This aspect ratio ranges from 0.15 to 0.25 (see Fig. 4d and Fig. S2 in ESI).

Fourth, the bending curvature varies greatly inside 4_1 knot. The two arms of the knot have the largest bending, while two boundaries and the middle segments of the knot have quite straight conformations. Detailed analysis of the bending variation within 4_1 knot will be presented in section of "**Variation of Tube Diameter and Bending inside the Knot Core**". Overall, the average knot conformation has a shape similar to the number of eight, and hence 4_1 knot is often called figure-eight knot. From the viewpoint of statistical physics, the average conformation in Fig. 4 can minimize the conformational free energy, which consists of two contributions: entropy and bending energy. The knot conformation tends to maximize the fluctuation around the average conformation (entropy) and minimize the bending energy. The competition of these two effects determines the average knot conformation.[40]

Tubes for Different Knot Sizes

Fig. 4 compares the 4_1 knot tubes for different knot sizes with a

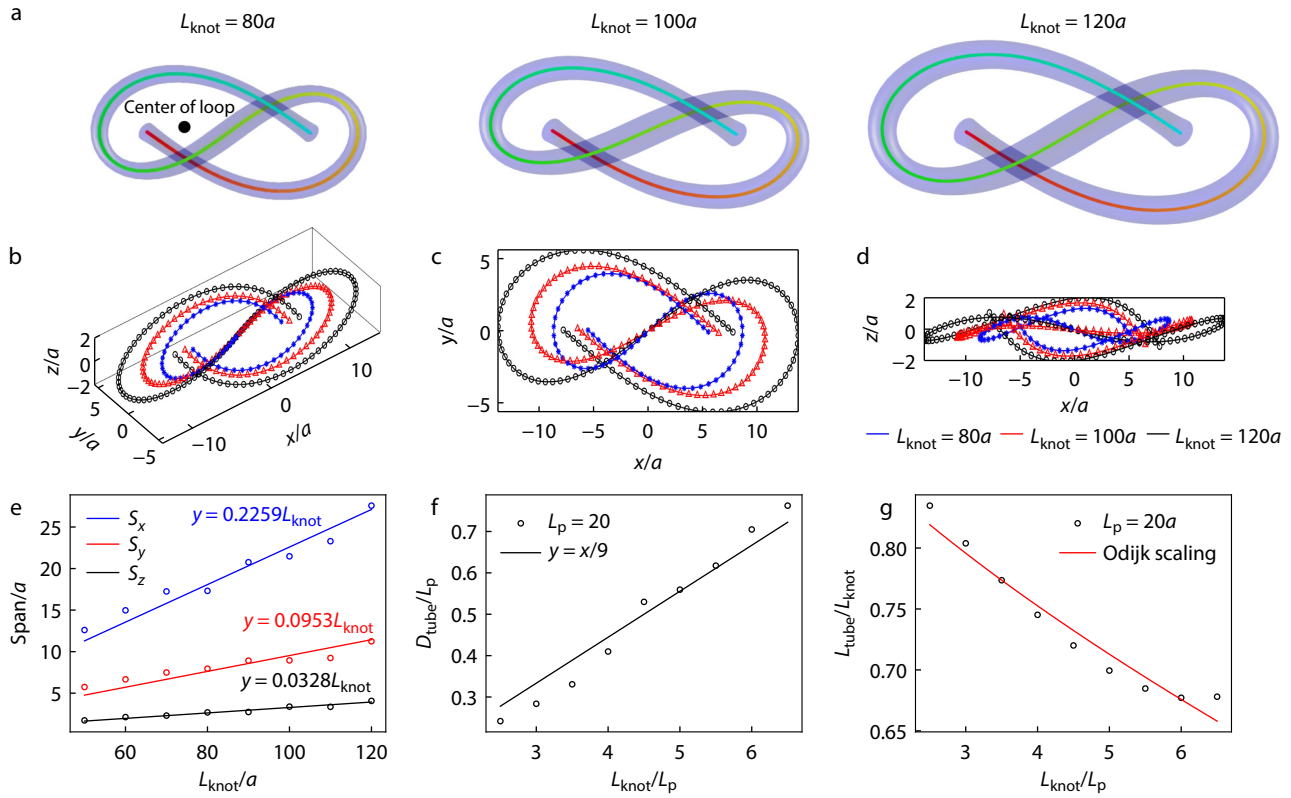

Fig. 4 Tubes for 4_1 knots with different knot sizes. (a) Knot tubes for three knot sizes. We fix the persistence length $L_p = 20a$. The tube axis corresponds to the average conformation. For better visualization, the tube diameters shown here are 0.2 times the actual tube diameters, D_{tube}. Here, D_{tube} is defined as twice the standard deviation of individual knot conformations around the average conformation. (b–d) Average knot conformations, *i.e.,* the tube axes, in 3D plot, *x*-*y* plane, and *x*-*z* plane, respectively. (e) The maximum span of the average conformation in three directions. (f) Average tube diameter as a function of the knot size. (g) Normalized length of the tube axis as a function of the knot size. The red line is calculated from Eq. (4).

fixed persistence length $L_p = 20a$. See more knot tubes in Figs. S3–S5 (in ESI). Here, the knot size is defined as the contour length inside the knot core. With the increase of the knot size from $80a$ to $120a$, the tube enlarges proportionally as indicated by the linear dependences on the max spans and the tube diameter on the knot size (Figs. 4e and 4f). We obtain the relationship between the tube diameter and the knot size:

$$D_{tube} \approx L_{knot}/9 \tag{3}$$

The coefficient 1/9 is an important parameter in the theoretical study of knots using the tube model,[37,38,40] because the knot conformational entropy strongly depends on tube diameter.

Fig. 4(g) shows the normalized length of the tube axis, L_{tube}, as a function of the knot size, L_{knot}. The relationship between L_{tube} and L_{knot} can be understood by considering a polymer confined in a tube with the polymer contour length as L_{knot} and the polymer extension along the tube axis as L_{tube}. Accordingly, we can relate L_{tube} and L_{knot} through the Odijk scaling:[56]

$$\frac{L_{tube}}{L_{knot}} \approx 1 - k_1\left(\frac{D_{tube}}{L_p}\right)^{\frac{2}{3}} \approx 1 - k_2\left(\frac{L_{knot}}{L_p}\right)^{\frac{2}{3}} \tag{4}$$

In the above equation, the first step is the original Odijk scaling, and the second step is based on the linear relationship between D_{tube} and L_{knot} in Eq. (3). Fig. 4(g) shows that the above equation agrees with the simulation results using a fitting parameter k_2=0.0982.

It is worth discussing the deviations of the knot behavior from the Odijk scaling. It is well-established that the Odijk scaling applies to straight tubes with solid tube walls and with a tube diameter smaller than the persistence length. The knot tube deviates from the tube in the Odijk scaling in three terms. First, the knot-tube axis is not straight but curved. The curvature becomes very significant for small knots. Our previous study has identified the knot scaling behavior changes when deceasing the knot size (see Fig. 2d of Ref.[40]). Second, the knot-tube diameter becomes larger than the persistence length for big knots. Third, the knot-tube walls are not solid but made of sparse polymer segments. Due to these three deviations, it is not surprising that the numerical results of knot tube do not exactly follow the Odijk scaling in Fig. 4(g) and other figures. Nevertheless, the Odijk scaling provides a very useful framework to understand the effect of the knot-tube confinement.

Tubes for Different Persistence Lengths

Fig. 5 compares the 4_1 knot tubes for different chain persistence lengths with a fixed knot size $L_{knot} = 100a$. See the coordinates of a knot tube in the ESI. With the increase of the persistence length from $L_p = 5a$ to $10a$, the maximum spans of the tube, S_x, S_y, and S_z, become larger (Fig. 5e) and the length of tube axis,

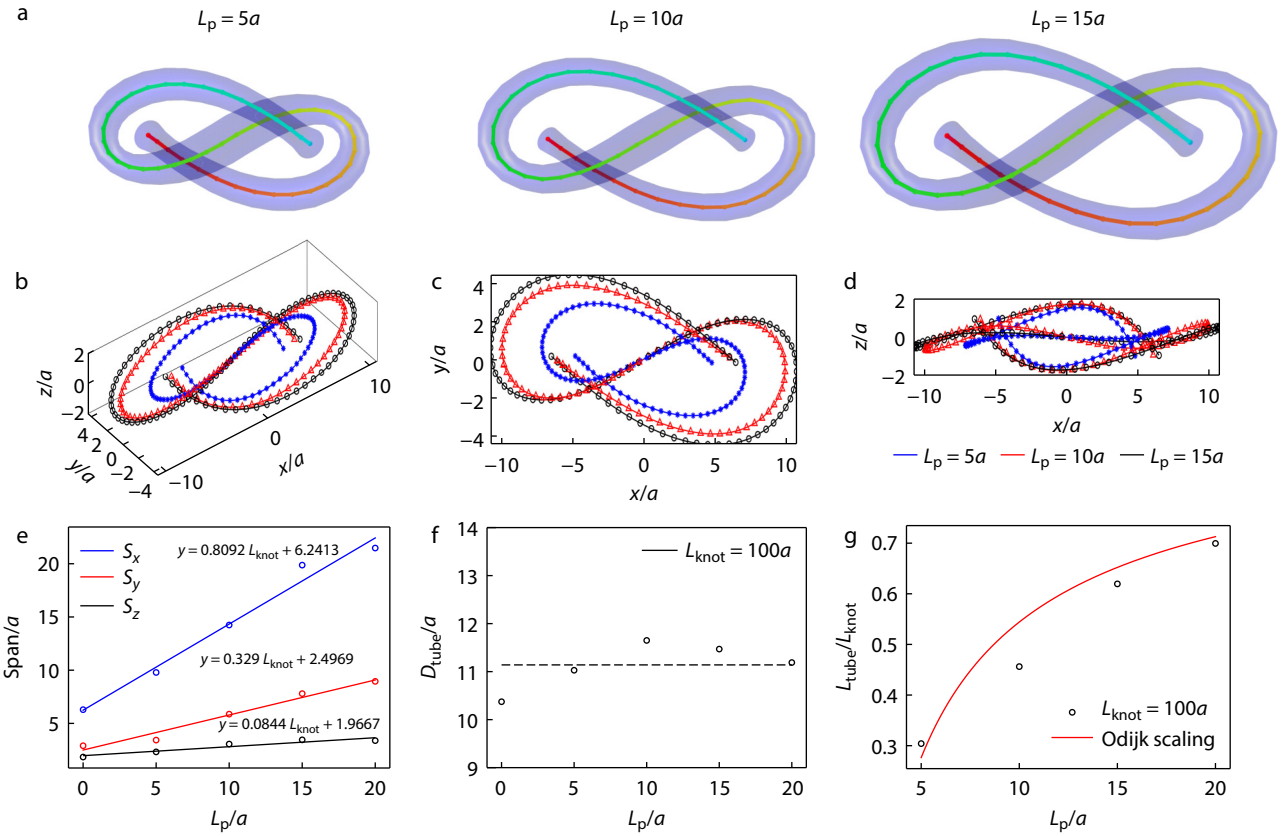

Fig. 5 Tubes for 4_1 knots with different persistence length. (a) Tubes for different persistence lengths. We fix the knot size L_{knot}=100a. Tube diameters are scaled down by a factor of 0.2 for better visualization. (b–d) Average knot conformations, *i.e.,* the tube axes, in 3D plot, *x*-*y* plane, and *x*-*z* plane, respectively. (e) The span of the mean conformation in the *x*, *y*, and *z* direction. (f) Average tube diameter as a function of the persistence length. (g) Normalized length of the tube axis as a function of the persistence length. The red line is calculated from Eq. (4).

L_{tube}, also become larger (Fig. 5g). However, the tube diameter is insensitive to L_p (Fig. 5f). In Fig. 5(g), the dependence of L_{tube} on L_p can be well explained by Eq. (4).

Variation of Tube Diameter and Bending inside the Knot Core

Fig. 6 shows the variations of tube diameter and bending inside 4_1 knot core. To facilitate the understanding of these variations, we divide the knot core into three regions: connection region, turning region, and threading region. To form a 4_1 knot, the polymer segments at the right side first generate a sharp-turn loop (turning region) and then thread through the loop on the left side (threading region). Symmetrically, the polymer segments at the left side first generate a sharp-turn loop and then thread through the loop on the right side. The left part and right part are connected by the connection region.

As shown in Fig. 6(a), the knot-core boundaries have the smallest tube diameters, which means that the polymer segments at the knot-core boundaries have the smallest fluctuation. A similar result has been observed for 3_1 knot: the smallest tube diameter also locates at the knot-core boundaries.[40] It is because the threading region is very close to the connection region in 3D space. A large spacing between the threading and connection region would increase the bending energy and hence is not favorable. Fig. 6(c) shows the radius of curvature, R_c, of the tube axis. As expected, the turning region has the sharpest bending, *i.e.* the smallest R_c.

Negative Extra Bending at Knot-Core Boundaries

Fig. 6(e) shows the average extra bending energy density of polymer segments within 4_1 knot core. We call it extra bending energy because we subtract the average bending energy density within the knot core, *e.g.,* the red segment in Fig. 6(f), by the average bending energy density in the unknotted region, *e.g.,* the blue segments in Fig. 6(f). The definition of the average extra energy is

$$\Delta E_{bend}^{knot} \equiv \langle E_{bend}^{knot} \rangle - \langle E_{bend}^{unknot} \rangle \quad (5)$$

A surprising result is that both knot-core boundaries have negative extra bending energy density, *i.e.,* the bending energy density at knot-core boundaries are even less than the unknotted region. Such negative values can be understood through the tube-confinement effect illustrated in Fig. 6(d). The tube confinement can suppress the bending of polymer segments within the tube. For example, when the tube diameter is zero, the polymer inside the tube has a straight conformation. Accordingly, the tube diameter can determine the reduction of polymer bending energy inside the tube. It is worth pointing out that the knot-tube axis is curved with a radius of curvature, R_c (Fig. 6d). Hence, both R_c and D_{tube} can determine polymer bending energy inside the tube. At knot-core boundaries, R_c is quite large and D_{tube} is quite small, both of which favors the negative value of ΔE_{bend}^{knot}. A physical understanding of the negative ΔE_{bend}^{knot} at knot-core bound-

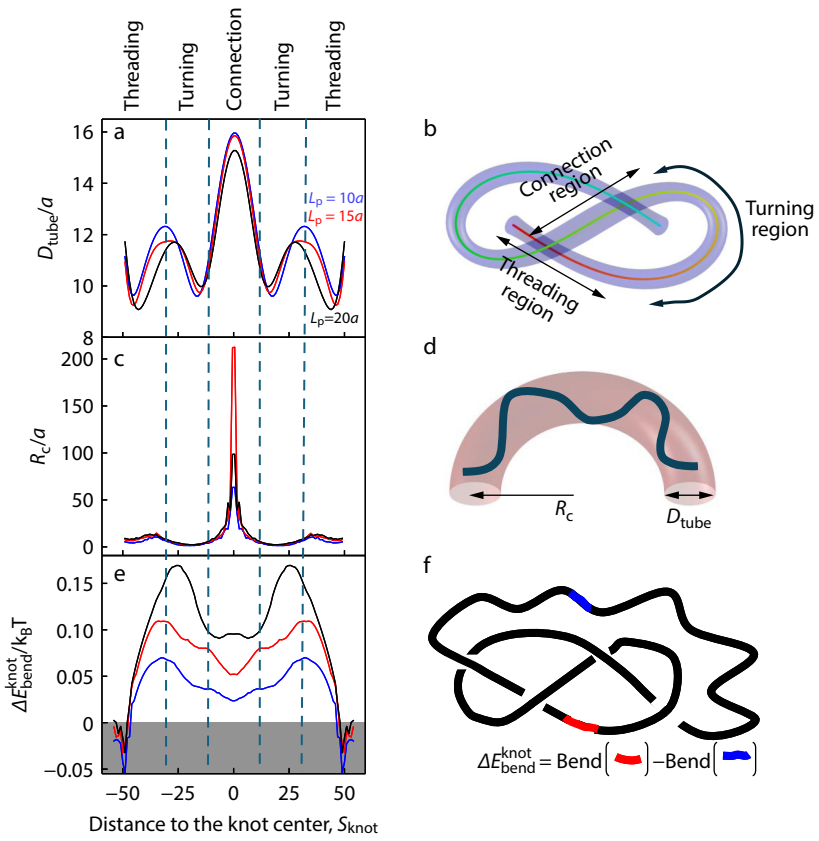

Fig. 6 Variations of tube diameter and curvature along the tube axis. (a) Tube diameters along the tube axis for L_{knot}=100a; (b) Labelling of three regions within the knot core; (c) Radius of curvature along the tube axis; (d) Illustration of a polymer confined in a curved tube which has a radius of curvature of R_c; (e) Extra bending energy along the tube axis; (f) Illustration of the extra bending energy.

aries is that the polymer segments at the threading region adopt rather straight conformations to gain more translational entropy, just like the polymers in liquid crystal.[56]

In Fig. 6(e), we notice that the extra negative bending region extends beyond the knot boundaries at s_{knot}= ±50a. Similar results were observed in our previous studies of 3_1 knots.[40] Such observation might be surprising, because one may expect that the knot core should be defined such that the bending inside the knot core is affected by knotting and the bending outside the knot core is not affected. Practically, the determination of the knot core is related to the end-closure method. To determine the knot core, we cut beads from both chain ends until the knot type changes. Every time we cut beads from chain ends, we need to close the two ends of this open chain by a loop and then calculate the Alexsander polynomial. The minimal inferring end-closure scheme appears to slightly underestimate the knot-core size (compared to the knot-core definition such that the bending inside the knot core is affected by knotting and the bending outside the knot core is not affected).[48] Such underestimation is probably because chain-end extension is applied in this end-closure method (see Fig. S7 in ESI). Such chain-end extension seems unavoidable when the chain ends are buried in conformations. The underestimation of knot-core size causes that the knot-core (Fig. 4a) is not exactly 4_1 knot, but looks like 2_2 knotoids.[57] After adding a short tail at each knot-core boundaries, the average conformation looks like 4_1 knot (see Fig. S9 in ESI).

It is important to note that the new algorithm developed in this work is used solely to align knot-core conformations. The new algorithm has nothing to do with the knot-core identification and the calculation of knot-core bending energy. It is also worth noting that simulation itself can only obtain the bending variation in the knot core, but cannot explain the bending variation, especially negative extra bending. To explain the bending variation, one must know tube diameter and tube-axis curvature, which can be only obtained after constructing knot tubes. It justifies the usefulness of the constructed knot tubes. In the above paragraphs, we suggest that tube-diameter narrowing in certain knot region causes less polymer bending in that region. It is also possible that less polymer bending in certain knot region causes tube-diameter narrowing. Distinguishing between these two scenarios may not be meaningful. The tube model is primarily a conceptual tool for visualizing irregular knot structures, as no physical tube actually exists. A rigorous theoretical approach would involve optimizing both the shape (or bending) and the tube diameter (fluctuation magnitude) to minimize free energy, which inherently couples these two factors. However, this approach is intractable. As an alternative, we develop a computational method to determine the shape (or bending) and tube diameter.

Results for Tubes and Bending of 5_1 and 5_2 Knots

We also construct tubes for 5_1 and 5_2 knots, similar to the

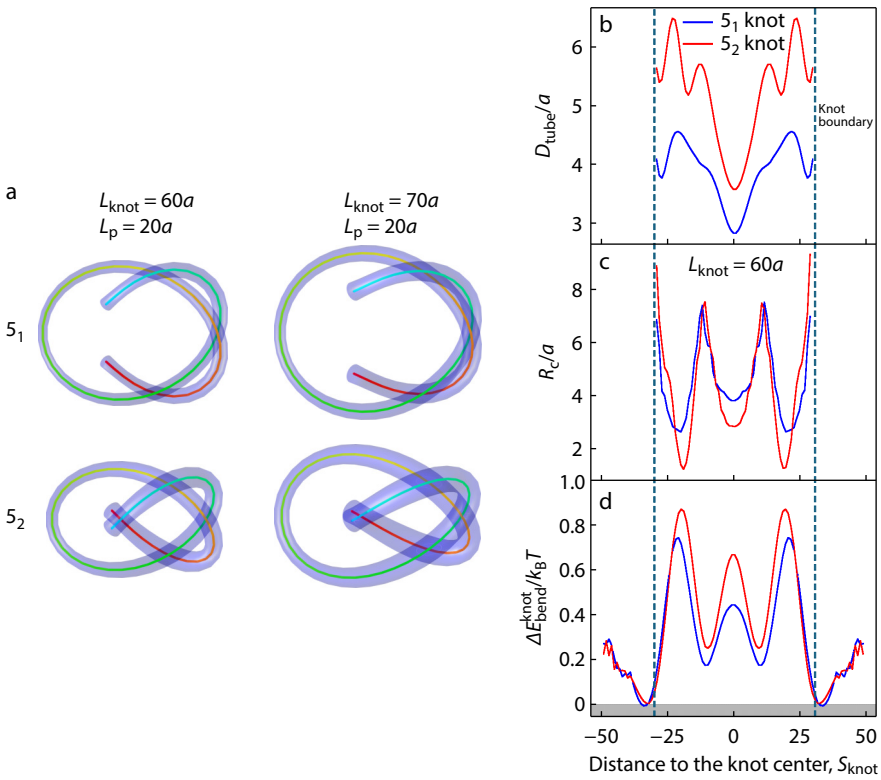

Fig. 7 (a) Constructed tubes for 5_1 and 5_2 knots. The tube diameters shown are 0.2 times of the actual tube diameters for easy visualization. (b–d) Tube diameter, curvature, and extra bending energy for 5_1 and 5_2 knots, similar to Fig. 6. The results are obtained from simulations with $L = 100a$ and $L_p = 20a$.

method for 4_1 knots, except for some modification for mirror-reflection operation (see Figs. S10 and S11 in ESI). The tubes are shown in Fig. 7(a). We also analyze the variation of tube diameters and curvature within the knot cores (Figs. 7b–7d), which can explain the least bending at knot boundaries. One reason why the extra bending does not go to negative value is that we use short chains $L = 100a$ in these simulations in order to speed up simulations and collect sufficient sampling for tube construction.

Negative Extra Bending of Entire Knotted Chains

In the above section, we analyze the extra bending energy at different sites within the knot core. In this section, we will present the results of extra bending energy of the entire knotted chain. We first calculate the average bending energy of the entire knotted chain. Then, we calculate the average bending energy of unknotted chain with the same chain length and same persistence length. Next, we calculate the difference, ΔE_{bend}^{knot}. Fig. 8 shows the simulation results of ΔE_{bend}^{knot}. In these simulations, we fix the chain length as $L = 300a$. When $L_p \lesssim 5a$, ΔE_{bend}^{knot} is negative, which means the knotted chain has less bending than the unknotted chain. The results are similar for three knot types: 4_1, 5_1 and 5_2. Similar results were observed before.[42] The reason why a smaller L_p promotes negative bending is as follows. The knot tube walls consist of monomers. The excluded volume interaction between monomers reduces the accessible tube diameter, *i.e.*, $D_{access} = D_{tube} - a$. The reduction in the accessible tube diameter can enhance the bending-suppression effect and favors negative bending. The reduction in the accessible tube diameter is stronger for smaller L_p. See more details in the previous study.[42]

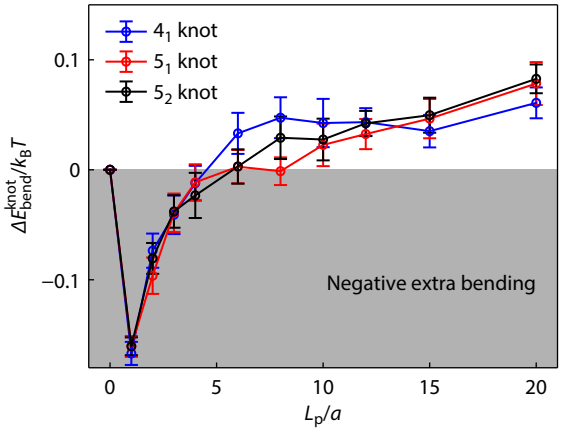

Fig. 8 Average excess bending energy as a function of persistence length for three knot types. Negative values of excess bending energy mean knotted polymers have less bending energy than unknotted polymers with the same length and same persistence length. The results from simulations of knotted and unknotted chains with $L = 300a$.

Knot Positioning Effect Caused by the Negative Extra Bending

The above results show that knot-core boundaries have negative extra bending, which means knot-core boundaries prefer straight conformations of polymer segments. Such preference

can lead to knot positioning effect for a polymer with non-uniform bending stiffness. The knot positioning effect refers to the situation where a knot prefers to stay at certain positions on the chain. Here, we consider a flexible knotted polymer with a stiff segment. It means all monomers are flexible except the stiff segment. For this polymer, the knot should prefer to place its boundary on the stiff segment.

Fig. 9 shows the favorable and unfavorable knot positions for a circular chain containing a 4_1, 5_1, or 5_2 knot. In all cases, the polymer is a flexible chain except a stiff segment with a persistence length of L_p^{stiff}. The circular chain length is $L = 300a$ and the length of stiff segment is L_{stiff}=2, 5, or 10a. In these simulations, we start with a knotted conformation and perform Langevin dynamics simulations. Bead-bead interactions are described by the Weeks-Chandler-Andersen potential,[53] which is nearly a hardcore repulsion. During the simulations, the knot diffuses along the chain.

To quantify the knot positioning effect, we calculate the distributions of knot positions during the simulations (Fig. 10). We define the knot position, x_{knot}, in a way such that x_{knot}=0 corresponds to the knot-core boundaries at the middle point of the stiff segment. Fig. 9 shows simulation snapshots and schematics for $x_{knot} \approx 0$ and $x_{knot} \gg 0$.

Fig. 10(a) shows the distributions of knot positions for 4_1 knot with $L_p^{stiff} = 5a$. The peak values at x_{knot}=0 are 1.5, 2.5, and 4.5 for $L_{stiff} = 2a$, $5a$, and $10a$, respectively. It means that the occurrences of x_{knot}=0 are 1.5, 2.5, or 4.5 times of other knot positions. Fig. 10(b) shows that increasing $L_p^{stiff} = 5a$ to $10a$ does not significantly enhance the knot-positioning effect, because the knot-positioning effect saturates at $L_p^{stiff} = 5a$. One can expect that when we decrease $L_p^{stiff} = 5a$ to 0, the knot-positioning disappears.

Figs. 10(c) and 10(d) show the knot-positioning effect for 5_1 and 5_2 knot, respectively. The peak values at x_{knot}=0 are similar among three knot types: 4_1, 5_1 and 5_2, which suggests that the knot-positioning effect is common for different knot types. It is quite possible that different knot types contain a threading region at the knot-core boundaries just like Fig. 6(b). The polymer segments in the threading region must adopt straight conformations no matter this polymer is flexible or stiff. Hence, it is more suitable to place stiff segments at knot-core boundaries. For comparison, forcing flexible segments to adopt straight conformations at knot-core boundaries will reduce the conformational entropy of this flexible segment and hence is unfavorable.

A similar positioning was observed in interlocked-ring polymers in a recent study by Luengo-Marquez, Assenza, and Micheletti.[58] When each polymer ring consists of a flexible segment and a rigid segment with the same length, they found the contact probability between rigid segments is much higher than the contact probability between flexible segments. They proposed an entropic reason to explain this effect: the contacts between flexible segments of mechanically bonded rings are entropically disfavored. It is quite possible that such contacts also force flexible segments to adopt relatively straight conformations.

Discussion about the Physical Meaning of Constructed Knot Tubes

In this section, we justify the physical meaning of our constructed knot tubes in the following terms. First, we do not specify a knotted curve and then construct a tube around it. Instead, we use an iterative procedure to determine the knotted curve (tube axis) and tube diameter. This iterative procedure is similar to searching the center point for a cluster of random points and

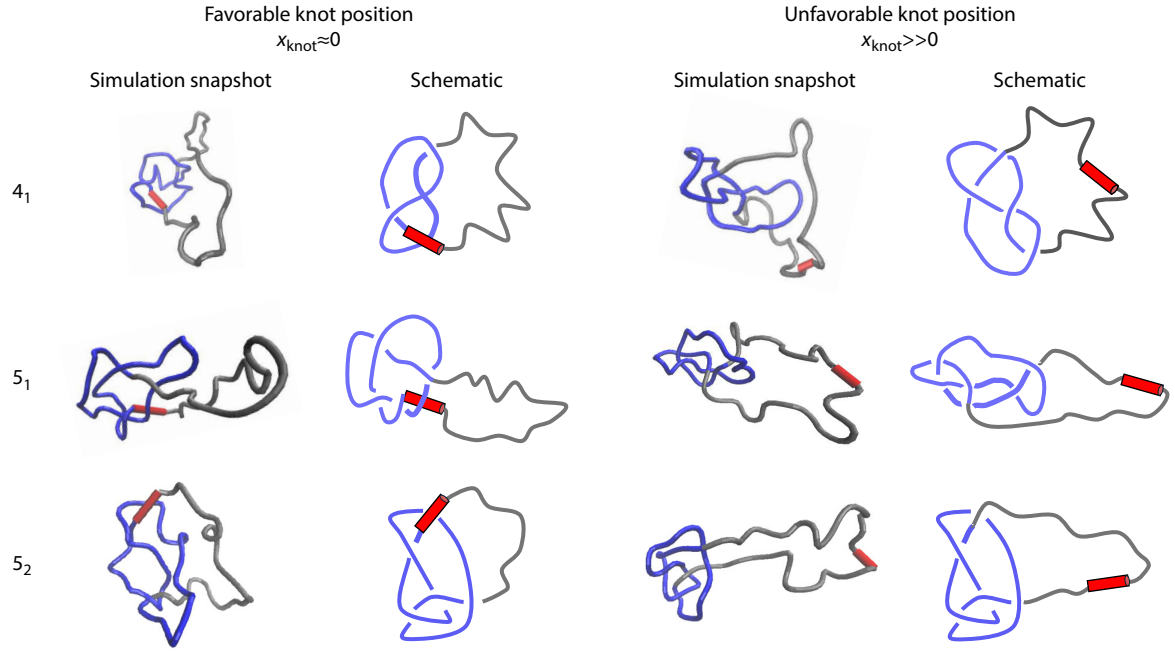

Fig. 9 Knot-positioning effect on a polymer with non-uniform bending stiffness. The polymer is flexible except for one stiff segment with a length of $L_{stiff} = 2a$, $5a$ or $10a$, and a persistence length of $L_p^{stiff} = 5a$, or $10a$. The 12 conformations are simulation snapshots and the corresponding schematics for 3 knot types. The stiff segments are labeled red, and the knot cores are labelled blue. x_{knot}=0 means one knot boundary is located at the middle of the stiff segment. The polymer length is 200a.

https://doi.org/10.1007/s10118-025-3405-8

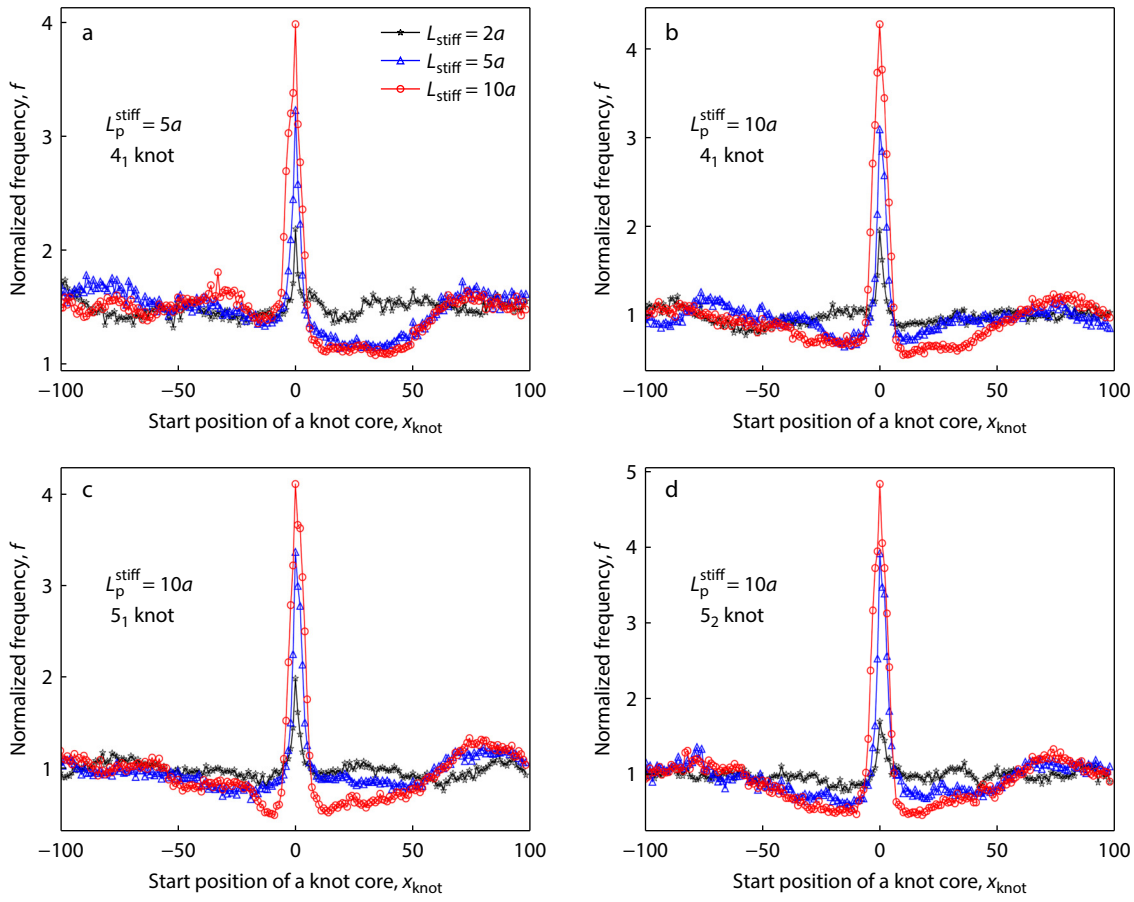

Fig. 10 Distribution of knot positions along a polymer. x_{knot}=0 means one knot boundary is located at the middle of the stiff segment. The four panels are from different knot types and different persistence lengths of the stiff segments. Three colors in each panel are for different lengths of the stiff segments. For the 4_1 knot, two different persistence lengths are considered: (a) $L_p^{stiff} = 5a$, (b) $L_p^{stiff} = 10a$, and for the (c) 5_1 knot and (d) 5_2 knot, a shared value is used: $L_p^{stiff} = 10a$ for both knots.

then calculating the standard deviation around this center point (see Fig. S12 in ESI). So, our algorithm to determine the knot tube is a natural method.

Second, our constructed knot tubes can quantitatively explain bending variation in the knot core, especially the negative extra bending at knot boundaries. The bending in different regions of knot core can be mapped to a chain in a curved tube with R_c and D_{tube}, both of which are determined from our constructed knot tubes. It has been proved that this mapping can quantitatively reproduce the bending in the knot core in our previous study.[42] Note that the negative extra bending is revealed by calculating the bending of individual knot conformations and has nothing to do with constructed knot tubes. So, reproduction of negative bending is an independent test for the correctness of the constructed knot tubes. If the constructed knot tubes are not physically correct, they cannot capture such subtle bending variation in the knot core.

Third, the shape of constructed 4_1 knot tubes is reasonable and can minimize the free energy cost, which results from the completion of bending energy and entropy. The knot tube consists of connection, turning and threading regions. The turning region primarily contributes to the bending, and the threading region primarily contributes to conformational entropy loss due to the intersection. The entropy would be increased by shifting the end of threading toward the center of loop, but such shifting also increases the bending. How the competition of entropy and bending leads to the average knot shape has been quantitatively analyzed in our previous study of 3_1 knot.[40]

CONCLUSIONS

In conclusion, we develop a new algorithm to construct the tubes for 4_1 knot. With these knot tubes and additional simulation analysis, we obtain many common properties for different knot types, including 4_1, 5_1, and 5_2 knots. We list the key findings in the following paragraphs.

First, constructing the tubes for 4_1 knot is more complicated than 3_1 knot. In the case of 3_1 knot, translation and rotation can properly align knot-core conformations. In the case of 4_1 knot, we must add mirror-reflection operation to properly align knot-core conformations. Proper alignment is required to preserve key structural features of a knot type. Otherwise, the average structure does not maintain the knot type.

Second, we obtain the average shape of 4_1 knot under thermodynamic equilibrium, which is different from the tight open 4_1 knot under tension,[55] or the circular tight 4_1 knot.

The average shape can be considered as an optimal structure to minimize the free energy of 4_1 knot, *i.e.,* the competition of bending energy and conformational entropy.

Third, bending curvature and structural fluctuation vary greatly among different sites in the knot core. There are some common variation patterns among different knot types. For example, both 3_1 and 4_1 knots have the smallest structural fluctuations on knot-core boundaries. The bending curvature and structural fluctuation are important structural features, which may be relevant for structural stability,[44,59,60] chemical catalysis,[32] and biological functions.[33]

Fourth, different knot types, including 3_1, 4_1, 5_1, 5_2 knots, have negative extra bending at knot-core boundaries. Negative extra bending means that the polymer bending caused by thermal fluctuations is suppressed at knot-core boundaries. This is because adopting straight conformations at knot-core boundaries can gain translational entropy in the threading region.

Fifth, bending energies of entire knotted chains are often less than the bending energies of unknotted chains with the same chain length and same persistence length when the persistence length is small ($L_p \lesssim 5a$). This counterintuitive phenomenon is because the virtual tube produced by knotting suppresses the bending in the knot core. We observe negative extra bending for different knot types, including 3_1, 4_1, 5_1, 5_2 knots, which suggests it may be a common phenomenon for all knot types.

Sixth, the knot-positioning effect is observed for different knot types, including 3_1, 4_1, 5_1, 5_2 knots. In this effect, a knot prefers to place its boundary at a stiff segment on a polymer with non-uniform bending stiffness.

Overall, the tube model is a promising theoretical model to gain valuable insights of different knot types, especially, the knot shape under thermodynamics equilibrium and magnitudes of structural fluctuations (tube diameters) in the knot core. Polymers with different knot types share many common properties, such as nearly straight conformations at knot-core boundaries. The structural features obtained from the tube model can be useful in understanding many knotting systems, such as DNA knots *in vivo*,[61] and in experiments. [13–16,18,21]

Conflict of Interests

The authors declare no interest conflict.

Electronic Supplementary Information

Electronic supplementary information (ESI) is available free of charge in the online version of this article at http://doi.org/10.1007/s10118-025-3405-8.

Data Availability Statement

The related data of this paper can be obtained from the author for reasonable reasons.

ACKNOWLEDGMENTS

This work was financially supported by the National Natural Science Foundation of China (No. 22273080) and Research Grants Council of Hong Kong (Nos. 11313322 and 11307224).

REFERENCES

1 De Gennes, P. Dynamics of entangled polymer solutions. I. The Rouse model. *Macromolecules* **1976,** *9*, 587−593.
2 Doi, M.; Edwards, S. F. *The Theory of Polymer Dynamics*. Oxford University Press: **1988** Vol. 73.
3 Yu, W. J.; Shen, G. C.; Zhou, X. W.; Li, M. Y.; Zhang, Y.; Zhou, H. M.; Li, D. Q. A constitutive model describing molecular configuration evolution and transient rheological behavior of entangled polymer solutions. *Chinese J. Polym. Sci.* **2021**, *39*, 1680−1694.
4 Peng, F.; Nie, C.; Xu, T. Y.; Sheng, J.F.; Chen, W.; Yu, W.C.; Li, L. B. Entanglement on nucleation barrier of polymer crystal. *Chinese J. Polym. Sci.* **2022**, *40*, 1640−1650.
5 Zhang, J. P.; Ma, L. C.; Ruan, Y. J.; Lu, Y. Y.; An, L. J. Evolution of polymer melt conformation and entanglement under high-rate elongational flow. *Chinese J. Polym. Sci.* **2024**, *42*, 2021−2029.
6 Micheletti, C.; Marenduzzo, D.; Orlandini, E. Polymers with spatial or topological constraints: theoretical and computational results. *Phys. Rep.* **2011**, *504*, 1−73.
7 Orlandini, E. Statics and dynamics of DNA knotting. *J. Phys. A* **2017**, *51*, 053001.
8 Virnau, P.; Kantor, Y.; Kardar, M. Knots in globule and coil phases of a model polyethylene. *J. Am. Chem. Soc* **2005**, *127*, 15102−15106.
9 Rubach, P.; Sikora, M.; Jarmolinska, A. I.; Perlinska, A. P.; Sulkowska, J. I. AlphaKnot 2.0: a web server for the visualization of proteins' knotting and a database of knotted AlphaFold-predicted models. *Nucleic Acids Res.* **2024**, *52*, W187−W193.
10 Jamroz, M.; Niemyska, W.; Rawdon, E. J.; Stasiak, A.; Millett, K. C.; Sułkowski, P.; Sulkowska, J. I. KnotProt: a database of proteins with knots and slipknots. *Nucleic Acids Res.* **2015**, *43*, D306−D314.
11 Tang, J.; Du, N.; Doyle, P. S. Compression and self-entanglement of single DNA molecules under uniform electric field. *Proc. Natl. Acad. Sci. U S A* **2011**, *108*, 16153−16158.
12 Renner, C. B.; Doyle, P. S. Stretching self-entangled DNA molecules in elongational fields. *Soft Matter* **2015**, *11*, 3105−3114.
13 Plesa, C.; Verschueren, D.; Pud, S.; van der Torre, J.; Ruitenberg, J. W.; Witteveen, M. J.; Jonsson, M. P.; Grosberg, A. Y.; Rabin, Y.; Dekker, C. Direct observation of DNA knots using a solid-state nanopore. *Nat. Nanotech.* **2016**, *11*, 1093−1097.
14 Amin, S.; Khorshid, A.; Zeng, L.; Zimny, P.; Reisner, W. A nanofluidic knot factory based on compression of single DNA in nanochannels. *Nat. Commun.* **2018**, *9*, 1506.
15 Klotz, A. R.; Soh, B. W.; Doyle, P. S. Motion of Knots in DNA Stretched by Elongational Fields. *Phys. Rev. Lett.* **2018**, *120*, 188003.
16 Sharma, R. K.; Agrawal, I.; Dai, L.; Doyle, P. S.; Garaj, S. Complex DNA knots detected with a nanopore sensor. *Nat. Commun.* **2019**, *10*, 4473.
17 Klotz, A. R.; Soh, B. W.; Doyle, P. S. An experimental investigation of attraction between knots in a stretched DNA molecule. *Europhys. Lett.* **2020**, *129*, 68001.
18 Ma, Z.; Dorfman, K. D. Diffusion of Knotted DNA Molecules in Nanochannels in the Extended de Gennes Regime. *Macromolecules* **2021**, *54*, 4211−4218.
19 Ma, Z.; Dorfman, K. D. Interactions between two knots in nanochannel-confined DNA molecules. *J. Chem. Phys*. **2021**, *155*, 154901.

20 Sharma, R. K.; Agrawal, I.; Dai, L.; Doyle, P.; Garaj, S. DNA knot malleability in single-digit nanopores. *Nano Lett.* **2021**, *21*, 3772–3779.
21 Mao, R.; Dorfman, K. D. Dynamics of double-knotted dna molecules under nanochannel confinement. *Macromolecules* **2024**, *57*, 5166–5174.
22 Song, X. Y.; Yang, Z. Y.; Yuan, Q. L.; Li, S. W.; Tang, Z. Q.; Dong, Y. T.; Jiang, S. C.; Xu, W. S. Understanding mass dependence of glass formation in ring polymers. *Chinese J. Polym. Sci.* **2023**, *41*, 1447–1461.
23 Arai, Y.; Yasuda, R.; Akashi, K. I.; Harada, Y.; Miyata, H.; Kinosita Jr, K.; Itoh, H. Tying a molecular knot with optical tweezers. *Nature* **1999**, *399*, 446.
24 Saitta, A. M.; Soper, P. D.; Wasserman, E.; Klein, M. L. Influence of a knot on the strength of a polymer strand. *Nature* **1999**, *399*, 46.
25 Zhang, M.; Nixon, R.; Schaufelberger, F.; Pirvu, L.; De Bo, G.; Leigh, D. A. Mechanical scission of a knotted polymer. *Nat. Chem*. **2024,** 16, doi: 10.1038/s41557-024-01510-3
26 Gong, H.; Li, J. F.; Zhang, H. D.; Shi, A. C. Force-extension curve of an entangled polymer chain: a superspace approach. *Chinese J. Polym. Sci.* **2021**, *39*, 1345–1350.
27 Rosa, A.; Di Ventra, M.; Micheletti, C. Topological jamming of spontaneously knotted polyelectrolyte chains driven through a nanopore. *Phys. Rev. Lett.* **2012**, *109*, 118301.
28 Suma, A.; Micheletti, C. Pore translocation of knotted DNA rings. *Proc. Natl. Acad. Sci. USA* **2017**, *114*, E2991.
29 Arsuaga, J.; Vázquez, M.; Trigueros, S.; Roca, J. Knotting probability of DNA molecules confined in restricted volumes: DNA knotting in phage capsids. *Proc. Natl. Acad. Sci. USA* **2002**, *99*, 5373–5377.
30 Marenduzzo, D.; Orlandini, E.; Stasiak, A.; Tubiana, L.; Micheletti, C. DNA-DNA interactions in bacteriophage capsids are responsible for the observed DNA knotting. *Proc. Natl. Acad. Sci. USA* **2009**, *106*, 22269–22274.
31 Lu, L.; Qiu, Q.; Lu, Y.; An, L.; Dai, L. Knotting in flexible-semiflexible block copolymers. *Macromolecules* **2024**, *57*, 5330–5339
32 Marcos, V.; Stephens, A. J.; Jaramillo-Garcia, J.; Nussbaumer, A. L.; Woltering, S. L.; Valero, A.; Lemonnier, J.-F.; Vitorica-Yrezabal, I. J.; Leigh, D. A. Allosteric initiation and regulation of catalysis with a molecular knot. *Science* **2016**, *352*, 1555–1559.
33 Christian, T.; Sakaguchi, R.; Perlinska, A. P.; Lahoud, G.; Ito, T.; Taylor, E. A.; Yokoyama, S.; Sulkowska, J. I.; Hou, Y.-M. Methyl transfer by substrate signaling from a knotted protein fold. *Nat. Struct. Mol. Biol.* **2016**, *23*, 941–948.
34 Hagita, K.; Murashima, T.; Sakata, N.; Shimokawa, K.; Deguchi, T.; Uehara, E.; Fujiwara, S. Molecular dynamics of topological barriers on the crystallization behavior of ring polyethylene melts with trefoil knots. *Macromolecules* **2022**, *56*, 15–27.
35 Yan, J.; Zhang, X.; Wang, J.; Hu, W. Effects of trefoil knots on the initiation of polymer crystallization. *Macromolecules* **2024**, *57*, 3914–3920.
36 Dong, Y. T.; Song, X. Y.; Xu, X.; Jiang, S.; Douglas, J. F.; Sun, Z. Y.; Xu, W. S. Glass formation in ring polymer melts having variable knot complexity and molecular mass. *Macromolecules* **2024**, *57*, 6875–6896.
37 Grosberg, A. Y.; Rabin, Y. Metastable tight knots in a wormlike polymer. *Phys. Rev. Lett.* **2007**, *99*, 217801.
38 Dai, L.; Renner, C. B.; Doyle, P. S. Metastable tight knots in semiflexible chains. *Macromolecules* **2014**, *47*, 6135–6140.
39 Grosberg, A. Y.; Feigel, A.; Rabin, Y. Flory-type theory of a knotted ring polymer. *Phys. Rev. E* **1996**, *54*, 6618.
40 Dai, L. Developing the tube theory for polymer knots. *Phys. Rev. Res.* **2020**, *2*, 022014.
41 Dai, L. Tube model for polymer knots with excluded volume interactions and its applications. *Macromolecules* **2021**, *54*, 9299–9306.
42 Lu, L.; Zhu, H.; Lu, Y.; An, L.; Dai, L. Application of the tube model to explain the unexpected decrease in polymer bending energy induced by knot formation. *Macromolecules* **2020**, *53*, 9443–9448.
43 Zhu, H.; Tian, F.; Sun, L.; Wang, S.; Dai, L. Revisiting the Non-monotonic Dependence of Polymer Knotting Probability on the Bending Stiffness. *Macromolecules* **2021**, *54*, 1623–1630.
44 Zhu, H.; Tian, F.; Sun, L.; Zhu, Y.; Qiu, Q.; Dai, L. Computational design of extraordinarily stable peptide structures through side-chain-locked knots. *J. Phys. Chem. Lett.* **2022**, *13*, 7741–7748.
45 Zhu, Y.; Zhu, H.; Tian, F.; Qiu, Q.; Dai, L. Quantifying the effects of slit confinement on polymer knots using the tube model. *Phys. Rev. E* **2022**, *105*, 024501.
46 Frank-Kamenetskiĭ, M.; Vologodskiĭ, A. Topological aspects of the physics of polymers: the theory and its biophysical applications. *Physics-Uspekhi* **1981**, *24*, 679–696.
47 Qiu, Q. Y.; Zhu, Y. J.; Wu, Z. T.; Dai, L. A simple and efficient algorithm to identify the chirality of polymer knots based on the alexander polynomial. *Chinese J. Polym. Sci.* **2024**, *42*, 2030–2037.
48 Tubiana, L.; Orlandini, E.; Micheletti, C. Probing the entanglement and locating knots in ring polymers: a comparative study of different arc closure schemes. *Prog. Theor. Phys. Suppl.* **2011**, *191*, 192–204.
49 Lawrence, J.; Bernal, J.; Witzgall, C. A purely algebraic justification of the Kabsch-Umeyama algorithm. *J. Res. Natl. Inst. Stand. Technol.* **2019**, *124*, 124028.
50 Plimpton, S. Fast parallel algorithms for short-range molecular dynamics. *J. Comput. Phys.* **1995**, *117*, 1–19.
51 Dai, L.; Soh, B. W.; Doyle, P. S. Effects of side chains on polymer knots. *Macromolecules* **2019**, *52*, 6792.
52 Dai, L.; Doyle, P. S. Universal knot spectra for confined polymers. *Macromolecules* **2018**, *51*, 6327–6333.
53 Weeks, J. D.; Chandler, D.; Andersen, H. C. Role of repulsive forces in determining the equilibrium structure of simple liquids. *J. Chem. Phys.* **1971**, *54*, 5237–5247.
54 Dai, L.; Renner, C. B.; Doyle, P. S. Metastable knots in confined semiflexible chains. *Macromolecules* **2015**, *48*, 2812–2818.
55 Pierański, P.; Przybył, S.; Stasiak, A. Tight open knots. *Eur. Phys. J. E* **2001**, *6*, 123–128.
56 Odijk, T. The statistics and dynamics of confined or entangled stiff polymers. *Macromolecules* **1983**, *16*, 1340–1344.
57 Goundaroulis, D.; Dorier, J.; Stasiak, A. A systematic classification of knotoids on the plane and on the sphere. *arXiv preprint arXiv:1902.07277* **2019**.
58 Luengo-Márquez, J.; Assenza, S.; Micheletti, C. Shape and size tunability of sheets of interlocked ring copolymers. *Soft Matter* **2024**, *20*, 6595.
59 Sułkowska, J. I.; Sułkowski, P.; Szymczak, P.; Cieplak, M. Stabilizing effect of knots on proteins. *Proc Natl Acad Sci* **2008**, *105*, 19714.
60 Sułkowska, J. I.; Sułkowski, P.; Szymczak, P.; Cieplak, M. Untying knots in proteins. *J. Am. Chem. Soc.* **2010**, *132*, 13954–13956.
61 Dean, F. B.; Stasiak, A.; Koller, T.; Cozzarelli, N. R. Duplex DNA knots produced by *Escherichia coli* topoisomerase I. Structure and requirements for formation. *J. Biol. Chem.* **1985**, *260*, 4975–4983.

https://doi.org/10.1007/s10118-025-3405-8